

---

# Discovery of annular X-ray emission centered on MAXI J1421–613: Dust-scattering X-rays?

Kumiko K. NOBUKAWA<sup>1</sup>, Masayoshi NOBUKAWA<sup>2</sup>, and Shigeo YAMAUCHI<sup>1</sup>

<sup>1</sup>Department of Physics, Faculty of Science, Nara Women's University, Kita-uoyanishi-machi, Nara, Nara 630-8506, Japan

<sup>2</sup>Faculty of Education, Nara University of Education, Takabatake-cho, Nara, Nara 630-8528, Japan

\*E-mail: kumiko@cc.nara-wu.ac.jp

Received (reception date); Accepted (acceptation date)

## Abstract

We report the discovery of an annular emission of  $\sim 3' - 9'$  radius around the center of a transient source, an X-ray burster MAXI J1421–613, in the Suzaku follow-up analysis. The spectrum of the annular emission shows no significant emission-line structure, and is well explained by an absorbed power law model with a photon index of  $\sim 4.2$ . These features exclude the possibility that the annular emission is a shell-like component of a supernova remnant. The spectral shape, the time history, and the X-ray flux of the annular emission agree with the scenario that the emission is due to a dust-scattering echo. The annular emission is made under a rare condition of the dust-scattering echo, where the central X-ray source, MAXI J1421–613, exhibits a short time outburst with three X-ray bursts and immediately re-enters a long quiescent period. The distribution of the hydrogen column density along the annular emission follows that of the CO intensity, which means that MAXI J1421–613 is located behind the CO cloud. We estimate the distance to MAXI J1421–613 to be  $\sim 3$  kpc assuming that the dust layer responsible for the annular emission is located at the same position as the CO cloud.

**Key words:** X-rays: bursts — X-rays: individual (MAXI J1421–613) — dust, extinction

---

## 1 Introduction

X-rays from an X-ray source are scattered by interstellar dust in the line of sight (Overbeck 1965). A dust-scattering halo is observed surrounding a bright X-ray source which is located behind a large amount of dusts. The dust-scattering halos provide information on the interstellar dust, such as the size distribution and composition of the grains (e.g., Predehl & Schmitt 1995, Draine 2003). By measuring the temporal variation of a halo, Predehl et al. (2000) constrained a line of sight position of Cygnus X-3.

If the X-ray emission with a short duration time is scattered by dust clouds, ring echoes are detected. Such samples have been detected around several gamma-ray bursts (e.g., Vaughan et al. 2004; Vaughan et al. 2006; Tiengo & Mereghetti 2006; Vianello et al. 2007; Pintore et al. 2017) and Galactic sources (e.g., Svirski et al. 2011; Mao et al. 2014). Only three Galactic samples have clear, well-defined, and large rings with a several arcminute scale (e.g., 1E 1547.0–5408, Circinus X-1, and V404 Cygni; Tiengo et al. 2010; Heinz et al. 2015; Vasilopoulos & Petropoulou 2016; Heinz et al. 2016). Most samples are accompanied with multiple rings, and each ring corresponds to a different dust layer or a different outburst. The thickness of the observed rings are different according to the situation; they reflect the duration time of the burst, the thickness of the dust layer, and the spatial resolution of the observation instrument.

An outburst of the new X-ray source MAXIJ1421–613 was detected by the MAXI Nova Alert System (Negoro et al. 2010) on 2014 January 9 (Morooka et al. 2014). During the outburst, MAXIJ1421–613 showed at least three type I X-ray bursts, and thus it is categorized into a neutron-star low-mass X-ray binary (Bozzo et al. 2014; Serino et al. 2015). The first burst with the observed flux of  $1.7 \times 10^{-9}$  erg cm<sup>-2</sup> s<sup>-1</sup> in the 3–10 keV band was detected on January 10 and lasted about 20 s (Bozzo et al. 2014). The second one occurred on January 16 is the brightest among the three. The bolometric flux was calculated to be  $7 \times 10^{-8}$  erg cm<sup>-2</sup> s<sup>-1</sup> and the duration time was about 36 s (Serino et al. 2015). The third one observed on January 18 has the bolometric flux of  $3.2 \times 10^{-8}$  erg cm<sup>-2</sup> s<sup>-1</sup> and the duration time of about 40 s (Serino et al. 2015).

After the MAXI alert, the Swift X-Ray Telescope (XRT) began a target-of-opportunity observation on the same day and observed the source approximately every 2 days until February 3. Suzaku performed a follow-up observation since January 31, and the observation continued for three days. But it did not detect the source and thus the  $3\sigma$  upper limit of the source flux of  $1.2 \times 10^{-13}$  erg cm<sup>-2</sup> s<sup>-1</sup> (0.5–10 keV) was obtained (Serino et al. 2015). Chandra also observed

MAXI J1421–613 on February 8 with the effective time of 969 s. No source was detected significantly, and the 95%-confidence upper limit on the flux was measured to be  $8.1 \times 10^{-14}$  erg cm $^{-2}$  s $^{-1}$  (0.2–10 keV; Chakrabarty et al. 2014).

Serino et al. (2015) analyzed the spectra during the outburst by utilizing the MAXI Gas Slit Camera (GSC) and the Swift XRT follow-up observations. The authors revealed that the spectra during the outburst can be explained by thermal Comptonization of multi-color disk blackbody emission. The photon index  $\Gamma \sim 2$  is a typical for low-mass X-ray binaries and remains almost constant during the outburst. Assuming the empirical maximum luminosity of X-ray bursts, Serino et al. (2015) estimated the maximum distance to be 7 kpc from the observed peak flux.

In this paper, we report on the discovery of an annular X-ray emission around MAXI J1421–613 from the Suzaku data. Based on spectral and radial profile analyses of the annular emission, we discuss its possible origin: (1) a supernova remnant or (2) a dust-scattering echo.

## 2 Observations and data reduction

We utilized the X-ray Imaging Spectrometer (XIS) data (Koyama et al. 2007) aboard Suzaku (Mitsuda et al. 2007). The XIS consists of four X-ray CCD cameras, each placed on the focal plane of the X-Ray Telescope (XRT; Serlemitsos et al. 2007). A field of view (FOV) of the XIS is  $17'8 \times 17'8$ . Three of the sensors (XIS0, 2, and 3) employ front-illuminated (FI) CCDs, while the other (XIS1) has a back-illuminated (BI) CCD. The entire region of XIS2 and one-fourth of XIS0 have been out of function since 2006 November and 2009 June, respectively.

We analyzed data with the analysis software package HEASoft 6.22.1 and the Suzaku calibration database (CALDB) released in 2016 February. The spectral analysis was performed with XSPEC 12.9.1. The data were screened by the standard event selection criteria for the XIS data processing. The response file (arf) and redistribution file (rmf) were produced by `xissimarfgen` and `xisrmfgen` (Ishisaki et al. 2007), respectively. The non-X-ray background (NXB) was estimated by `xisnxbgen` (Tawa et al. 2008) and was subtracted from spectra and images in the following analysis. For the spectral analysis, we used nearby blank-sky data as background. The observation log is summarized in table 1. Throughout the paper, FI and BI spectra were fitted simultaneously, but only the FI spectra (XIS0+3) are displayed in the figures for brevity. Error bars given in figures show the  $1\sigma$  statistical errors.

**Table 1.** Observation log.

Object Name	Obs.ID	Pointing direction		Observation date (UT)		Exposure (ks)
		$\alpha_{J2000.0}$ ( $^{\circ}$ )	$\delta_{J2000.0}$ ( $^{\circ}$ )	Start	End	
MAXIJ1421–613	908003010	215.40	–61.61	2014-01-31 12:20:40	2014-02-03 14:00:17	48.8
ASO0304 (background)	504054010	213.34	–62.08	2009-07-24 21:42:28	2009-07-26 03:29:22	44.2

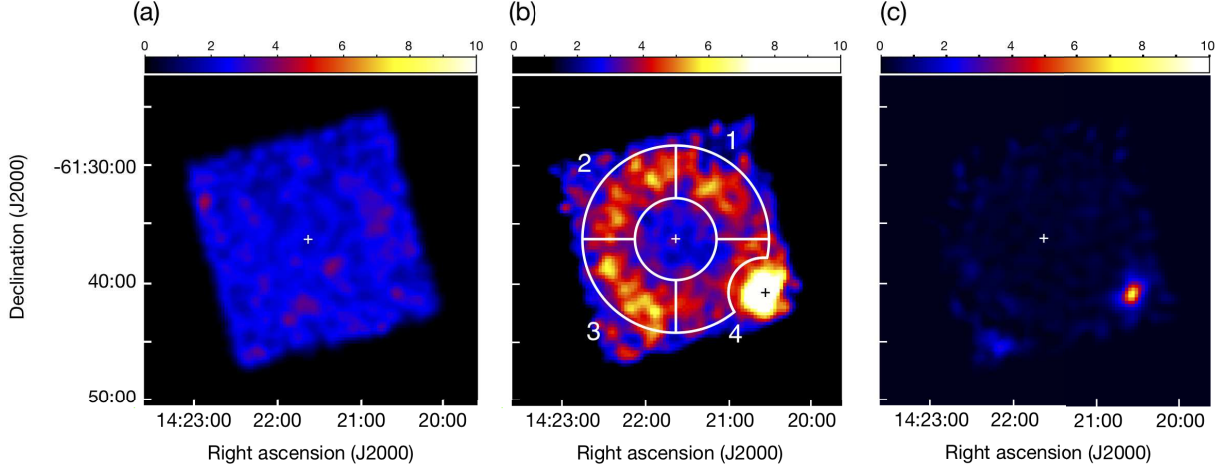


**Fig. 1.** X-ray images of the XIS FOV containing MAXIJ1421–613 in the 0.5–2 keV (a), 2–5 keV (b), and 5–8 keV bands (c). The color scales are shown in the arbitrary unit. A white cross in (b) shows the position of MAXIJ1421–613, while a black cross shows Suzaku J1420.5–6141 (see text). We extracted a source spectrum from the whole annular region surrounded by the white lines. We divided the annular region into the four parts (1–4) and also performed spectral analysis for each quadrant.

### 3 Analysis and Results

The X-ray images of the entire FOV of Suzaku XIS in the 0.5–2 keV, 2–5 keV and 5–8 keV bands are given in figure 1, where the position of MAXIJ1421–613 is shown by the white cross. No significant X-ray emission was found at this position. Another point source was found (black cross in figure 1) at the position of  $(\alpha, \delta)_{J2000.0} = (14^{\text{h}}20^{\text{m}}34^{\text{s}}07, -61^{\circ}41'00''.33)$  with the positional uncertainty of  $19''$  (Uchiyama et al. 2008). No catalogued source has been reported so far at this position, hence is newly named as Suzaku J1420.5–6141. The spectrum of Suzaku J1420.5–6141 was made from a circle with a radius of  $3'$ . The best-fit power-law model gave absorption column density, photon index, and observed flux in the 2–10 keV band to be  $N_{\text{H}} = 4.0^{+0.9}_{-0.8} \times 10^{22} \text{ cm}^{-2}$ ,  $\Gamma = 1.6 \pm 0.3$ , and  $F_{2-10 \text{ keV}} = (1.4 \pm 0.1) \times 10^{-12} \text{ ergs cm}^{-2} \text{ s}^{-1}$ , respectively. No time variability within  $< 10\%$  was found.

We found clear an annular emission around MAXIJ1412–613. The width is about  $6'$  and the flux is reasonably high with uniform distribution except Suzaku J1420.5–6141. The spectrum was made from the annular region excluding Suzaku J1420.5–6141. The background spectrum was obtained from the nearby position (table 1). These spectra are shown in figure 2.

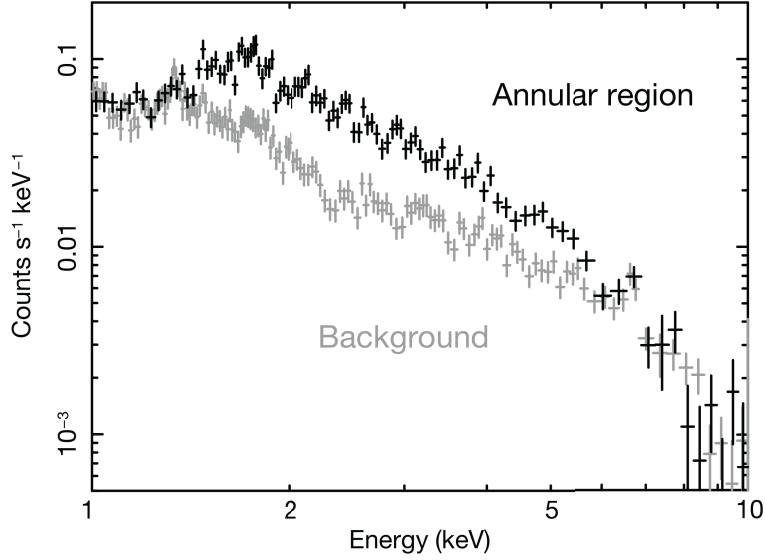


**Fig. 2.** Source spectrum (black) extracted from the whole annular region indicated by white lines in figure 1(b) and background spectrum (gray) extracted from the blank-sky data.

**Table 2.** Best-fit parameters of the annular emission spectrum\*.

Parameter	phabs×apec	phabs×power-law
$N_{\text{H}}(10^{22} \text{ cm}^{-2})$	$2.3 \pm 0.3$	$3.7 \pm 0.5$
$\Gamma$	–	$4.2 \pm 0.3$
$kT$ (keV)	$1.4 \pm 0.2$	–
Abundance (solar)	$< 0.09$	–
Flux <sup>†</sup>	$1.9 \pm 0.1$	$2.5 \pm 0.1$
reduced $\chi^2$ (d.o.f.)	1.17 (112)	1.09 (113)

\* Errors are quoted at the 90% confidence levels.

<sup>†</sup> Unabsorbed values in the 2–5 keV band in unit of  $10^{-12} \text{ erg cm}^{-2} \text{ s}^{-1}$ .

The background subtracted spectrum was fitted with either a phenomenological power-law model or an optically thin thermal plasma model. The best-fit results are given in table 2. The hydrogen column density obtained by the power-law model is  $N_{\text{H}} = (3.7 \pm 0.5) \times 10^{22} \text{ cm}^{-2}$ , which is consistent with that of MAXI J1412–613 measured by Serino et al. (2015),  $N_{\text{H}} = 4.8_{-1.1}^{+1.3} \times 10^{22} \text{ cm}^{-2}$ .

The region of the annular emission is shown on the flux map of CO (Dame et al. 2001) in figure 3. Referring the  $N_{\text{H}}$  distribution, we divided the region into four quadrants (quadrant 1–4). The spectrum of each quadrant was fitted with a phenomenological power-law model. The photon indices of the four parts are consistent with the best-fit value of the whole annular emission ( $\Gamma = 4.2$ ) within the 90% confidence levels. We fixed the photon index to  $\Gamma = 4.2$  and made other parameters free. The best-fit  $N_{\text{H}}$  values are  $4.5 \pm 0.4$ ,  $3.7 \pm 0.4$ ,  $3.1 \pm 0.3$ , and

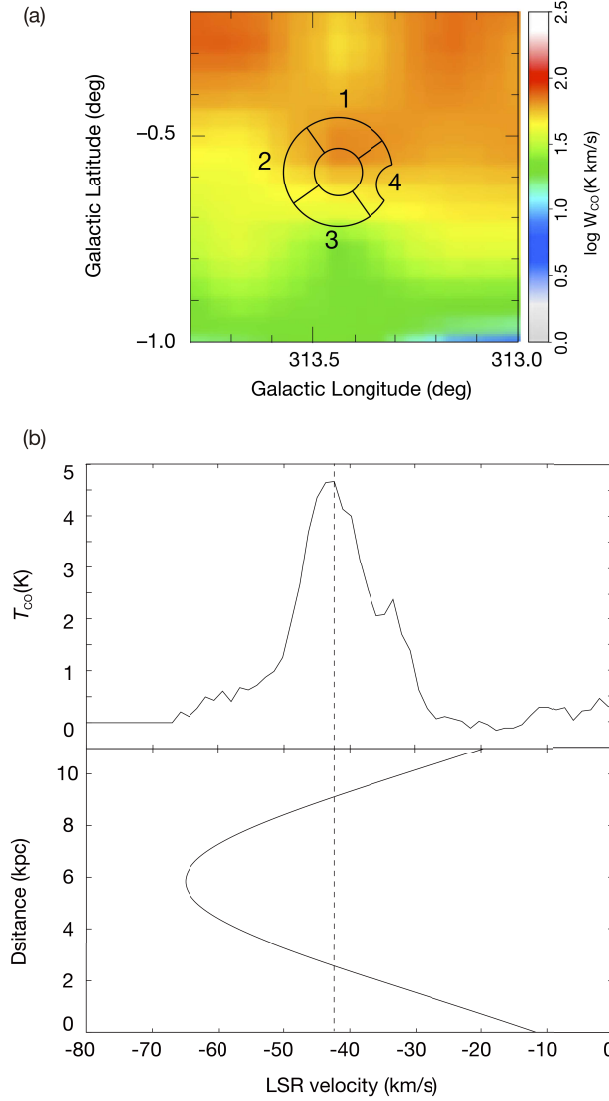


**Fig. 3.** (a) CO map around MAXIJ1421–613 (Dame et al. 2001). The quadrants of the annular region are overlaid. (b) (Top) CO spectrum in the direction of the quadrant 1 taken from Dame et al. (2001). Dashed line indicates the spectral peak at  $\sim 43 \text{ km s}^{-1}$ . (Bottom) Correlation between distance from the sun and radial velocity (LSR) in a direction of quadrant 1 ( $l = 313.^\circ 4$ ) inferred from the Galactic rotation curve obtained by McClure-Griffiths & Dickey (2007).

$3.2 \pm 0.4$  in the unit of  $10^{22} \text{ cm}^{-2}$  for the quadrant 1, 2, 3, and 4, respectively. The largest  $N_{\text{H}}$  at the quadrant 1 corresponds to the CO peak, while the smallest  $N_{\text{H}}$  at quadrant 3 is out of the CO peak (Dame et al. 2001).

In order to give a constraint on the cloud position, adopting the Galactic rotation curve by McClure-Griffiths & Dickey (2007) of  $R_o = 8.5 \text{ kpc}$  and  $V_o = 220 \text{ km s}^{-1}$ , we plotted the correlation map of the LSR velocity and the distance from the sun (see figure 3). The LSR of  $\sim 43 \text{ km s}^{-1}$  gives two solutions for the distance of the cloud of  $\sim 2.6 \text{ kpc}$  and  $\sim 9 \text{ kpc}$ .

We made four annular spectra of  $3'5-5'$ ,  $5'-6'$ ,  $6'-7'$ , and  $7'-8'$  and investigated spectral

**Table 3.** Best-fit parameters of each period spectrum\*.

	period 1	period 2	period 3
Start time (UT)	2014-01-31 12:20:40	2014-02-01 13:47:37	2014-02-02 15:37:31
Exposure time (ks)	17.1	15.2	16.4
Parameter	phabs×power-law		
$N_{\text{H}}(10^{22} \text{ cm}^{-2})$	3.7 (fixed)	3.7 (fixed)	3.7 (fixed)
$\Gamma$	$4.2 \pm 0.2$	$4.3 \pm 0.2$	$4.1 \pm 0.2$
Flux <sup>†</sup>	$2.6 \pm 0.1$	$2.4 \pm 0.1$	$2.2 \pm 0.1$
reduced $\chi^2$ (d.o.f.)	1.11 (79)	1.24 (69)	0.96 (69)

\* Errors are quoted at the 90% confidence levels.

† Unabsorbed values in the 2–5 keV band in unit of  $10^{-12} \text{ erg cm}^{-2} \text{ s}^{-1}$ .

variation with a radius. We fitted the spectra with the phenomenological power-law model with fixing the  $N_{\text{H}}$  value of  $3.7 \times 10^{22} \text{ cm}^{-2}$ . No clear differences in the spectral shape were found.

We also extracted spectra of the annular emission from the three periods and examine the spectral change with time. The periods are named as period 1, 2 and 3 (see table 3). The spectrum was fitted with the phenomenological power-law model with fixing the  $N_{\text{H}}$  value of  $3.7 \times 10^{22} \text{ cm}^{-2}$ . The best-fit spectral parameters are listed in table 3.

In order to examine the expansion of the annular emission, we made a radial profile from three different periods of the observation and fit the radial profiles with a gaussian. The gaussian centroid of period 1, 2, and 3 was measured to be  $5'.4 \pm 0'.2$ ,  $5'.9 \pm 0'.2$ , and  $5'.9 \pm 0'.3$ , respectively.

We also checked whether the annular emission is detected by other satellites. Swift performed two observations of MAXI J1421–613 with the Photon Counting (PC) mode in almost the same period as the Suzaku observations; one observation started on January 30 (Obs ID = 00033098009) and the other one started on February 1 (Obs ID = 00033098010). The total exposure time of the two observations is 2.4 ks. We extracted a radial profile centered on the position of MAXI J1421–613 in the 1–5 keV band using the Swift data. The number of counts in each radial bin are divided by the corresponding area. We also divided the profile by the effective exposure time derived from the exposure map in order to take in to account telescope vignetting, the CCD bad pixels and columns, and the attitude variations. We found that the profile has a hint of a peak at  $\sim 6'$ . The count rate of the annular emission is measured to be  $0.03\text{--}0.05 \text{ counts s}^{-1}$ , which approximately corresponds to the flux of  $(2\text{--}3) \times 10^{-12} \text{ erg cm}^{-2} \text{ s}^{-1}$ . These values are consistent with the radius and the flux of the annular emission observed by Suzaku. However, the swift data could not constrain the spectral parameters due to insufficient

statistics. We also checked the Chandra/ACIS-S data, but we cannot distinguish the annular emission due to a short exposure time (1 ks) and the low net counts of 68 within the whole FOV (the 2–5 keV band).

## 4 Discussion

### 4.1 Origin of the annular emission

We found an annular X-ray emission around the low-mass X-ray binary MAXI J1421–613 from the Suzaku data. We discuss its origin based on the results.

Composite type SNRs have a shock-heated thermal shell with a Compact Central Object (CCO) (e.g., CTB109, RCW103; Sasaki et al. 2004; Tuohy & Garmire 1980). The observed morphology indicates one possibility that the annular emission is the shock-heated shell of SNR with a CCO (MAXI J1421–613) in the center, where the CCO would be a neutron star of the low mass X-ray binary (X-ray burster). The flux and power-law index ( $\Gamma$ ) of MAXI J1421–613 during the outburst phase are  $10^{-9}$ – $10^{-10}$  erg cm $^{-2}$  s $^{-1}$  and  $\Gamma \sim 2.1$ , respectively (Serino et al. 2015). The value of  $\Gamma$  is consistent with a disk-blackbody model for a neutron star low-mass binary (Mitsuda et al. 1984).

The spectrum of the annular emission was nicely fitted with a power-law model with  $\chi^2/\text{d.o.f.} = 1.09$ . The spectrum shows no prominent line, setting the abundance upper-limit of  $< 0.09$  solar (table 2). Such low abundance is unreasonable for the ejecta or interstellar gas of SNRs. No radio shell has been reported. Thus, the annular emission would not be due to a thermal plasma in a composite type SNR. The power-law index of  $\Gamma \sim 4.2$  is out of the standard synchrotron radiation found in a shell region of SNRs ( $\Gamma \sim 2$ – $3$ , e.g., SN1006: Bamba et al. 2003; RX J1713–3946: Koyama et al. 1997). The mean flux of the annular emission,  $(2.5 \pm 0.1) \times 10^{-12}$  erg cm $^{-2}$  s $^{-1}$  (table 2), is less than the peak flux of MAXI J1421–613. These facts support that the annular emission is made by dust scattering.

The dust scattering echo has a halo-like profile in persistent bright point sources (e.g. many Galactic binaries, Predehl & Schmitt 1995), while a ring-like structure with many concentric sub-rings is found in highly variable X-ray sources, i.e. 1E1547.0–5408, Circinus X-1, and V404 Cygni (Tiengo et al. 2010; Xiang et al. 2011; Heinz et al. 2015; Heinz et al. 2016; Vasilopoulos & Petropoulou 2016). The differential cross section of X-ray dust scattering depends on the photon energy and is given by  $E^{-\Gamma}$  in the optically thin limit where one can approximate  $(1 - e^{-\tau})$  as  $\tau$ , where  $\tau$  is the opacity. The index  $\Gamma$  is about 2 (Draine 2003). The observed  $\Gamma$  of the annular emission is  $\sim 4.2$  which is larger than MAXI J1421–613 of  $\Gamma \sim 2.1$

by  $\Delta\Gamma \sim 2$  (Serino et al. 2015). This value strongly supports the dust scattering echo scenario.

If the annular emission is dust scattering of the short (but not instantaneous) outburst, the radius may expand with time. In fact, we found a hint of the radius expansion from  $\sim 5.4$  (period 1) to  $\sim 5.9$  (periods 2 and 3). We also found a hint of flux decrease from  $2.6 \times 10^{-11}$  erg cm $^{-2}$  s $^{-1}$  (period 1) to  $2.2 \times 10^{-11}$  erg cm $^{-2}$  s $^{-1}$  (period 3) without the spectral change. In the slight expansion of  $\sim 30''$ , the differential cross section of dust scattering shows a little decrease (Draine 2003). The time history is well consistent with those expected from the dust scattering echo scenario.

#### 4.2 Location of MAXI J1421–613 and dust layer

In this section, we estimate the distance to MAXI J1421–613 and a dust layer.

MAXI J1421–613 entered into an outburst phase around 2014 January 7 after a long period of quiescent phase and exhibited a flux peak with  $\sim 10^{-9}$  erg cm $^{-2}$  s $^{-1}$  around January 9–10 (see figure 2 in Serino et al. 2015). Then the intensity gradually decreased from January 10 to January 13, and reached a mean flux of  $\sim 10^{-10}$  erg cm $^{-2}$  s $^{-1}$  in the period of January 14 to January 19. Thus, we assume that light from the outburst phase made the annular emission: the outer region of the annular emission is occupied by the X-rays of earlier epoch, while the inner region is by the later epoch. Here, we also assume that the epoch of the flux peak on January 9 is corresponding to the brightest radius of  $6'$ . The Suzaku observations were carried out about 21–24 days after the epoch of the flux peak, and hence the difference in the light traveling times between the direct and the dust scattered lights would be about 21–24 days.

As is shown in section 3, MAXI J1421–613 is located behind the  $43$  km s $^{-1}$  CO molecular cloud. The LSR of  $\sim 43$  km s $^{-1}$  gives two solutions for the distance of the molecular cloud of  $\sim 2.6$  kpc and  $\sim 9$  kpc. The distance to MAXI J1421–613 can be calculated using the difference in the light traveling times, the distance to the dust layer, and the width of the annular emission (equation 8 in Trümper & Schönfelder 1973). We assume that the dust layer responsible for the annular emission is located at the same position as the CO cloud, namely 2.6 kpc or 9 kpc. If the dust layer is located at 2.6 kpc from the Sun, the distance to MAXI J1421–613 is calculated to be 3 kpc. In the case of 9 kpc, the distance to MAXI J1421–613 is calculated to be 30 kpc, which is beyond the Galaxy, and thus unlikely.

We propose that the distance to MAXI J1421–613 is 3 kpc on the assumption that the dust layer lies at the same position as the  $43$  km s $^{-1}$  CO molecular cloud. This demonstrates that they are located at the Scutum-Centaurus arm in the Galaxy. In the cases, the radius

expansion of the annular emission is consistent with the value during the Suzaku observations ( $\sim 30''$  per 3 days, see section 3).

## 5 Conclusion

We note that the preceding analysis with Suzaku by Serino et al. (2015) failed to find the annular emission, and hence the present paper reports the new discovery of the annular emission. Our detection of the annular emission with no bright point source (figure 1) catches very rare chance of the dust scattering echo; MAXI J1421–613 showed an outburst phase ( $10^{-9}$ – $10^{-10}$  erg cm $^{-2}$  s $^{-1}$ ) within a short duration of  $< 10$  days whereas the scattered X-rays are observed after MAXI J1421–613 re-entered to a long quiescent phase ( $< 10^{-13}$  erg cm $^{-2}$  s $^{-1}$ ). The steeper  $\Gamma$  of the annular emission of  $\sim 4.2$  than that of MAXI J1421–613 of  $\sim 2.1$ , and the time history of the radius and the flux is all consistent with a dust scattering echo. If MAXI J1421–613 shows an outburst again, one would be able to observe a dust scattering echo when they observe the object more than ten days after the outburst.

## Acknowledgments

We thank all the members of the Suzaku and MAXI teams. We are grateful to Dr. Katsuji Koyama and Dr. Yasuharu Sugawara for their valuable comments. K.K.N. is supported by Research Fellowships of JSPS for Young Scientists. This work was supported by JSPS and MEXT KAKENHI Grant Numbers JP16J00548 (KKN) and JP17K14289 (MN).

## References

- Bamba, A., Yamazaki, R., Ueno, M., & Koyama, K. 2003, *ApJ*, 589, 827
- Bozzo, E. et al. 2014, *Astronomer’s Telegram*, 5765
- Chakrabarty, D., Jonker, P. G., & Markwardt, C. B. 2014, *Astronomer’s Telegram*, 5894
- Dame, T. M., Hartmann, D., & Thaddeus, P. 2001, *ApJ*, 547, 792
- Draine, B. T. 2003, *ApJ*, 598, 1026
- Heinz, S. et al. 2015, *ApJ*, 806, 265
- Heinz, S., Corrales, L., Smith, R., Brandt, W. N., Jonker, P. G., Plotkin, R. M., & Neilsen, J. 2016, *ApJ*, 825, 15
- Ishisaki, Y. et al. 2007, *PASJ*, 59, S113
- Koyama, K., Kinugasa, K., Matsuzaki, K., Nishiuchi, M., Sugizaki, M., Torii, K., Yamauchi, S., & Aschenbach, B. 1997, *PASJ*, 49, L7

Koyama, K., Tsunemi, H., Dotani, T., et al. 2007, PASJ, 59, S23

Mao, J., Ling, Z., & Zhang, S.-N. 2014, ApJ, 785, 23

McClure-Griffiths, N. M., & Dickey, J. M. 2007, ApJ, 671, 427

Mitsuda, K. et al. 1984, PASJ, 36, 741

Mitsuda, K. et al. 2007, PASJ, 59, S1

Morooka, Y., et al. 2014, Astronomer's Telegram, 5750

Negoro, H., et al. 2010, in ASP Conf. Ser., 434, Astronomical Data Analysis Software and Systems XIX, ed. Y. Mizumoto et al. (San Francisco: ASP), 127

Overbeck, J. W. 1965, ApJ, 141, 864

Pintore, F., et al. 2017, MNRAS, 472, 1465

Predehl, P., & Schmitt, J. H. M. M. 1995, A&A, 293, 889

Predehl, P., Burwitz, V., Paerels, F., & Trümper, J. 2000, A&A, 357, L25

Sasaki, M., Plucinsky, P. P., Gaetz, T. J., Smith, R. K., Edgar, R. J., Slane, P. O. 2004, ApJ, 617, 322

Svirski, G., Nakar, E., & Ofek, E. O. 2011, MNRAS, 415, 2485

Serino, M. et al. 2015, PASJ, 67, 30

Serlemitsos, P. J. et al. 2007, PASJ, 59, S9

Tawa, N. et al. 2008, PASJ, 60, S11

Tiengo, A., & Mereghetti, S. 2006, A&A, 449, 203

Tiengo, A. et al. 2010, ApJ, 710, 227

Trümper, J & Schönfelder, V, 1973, A&A, 25, 445

Tuohy, I. and Garmire, G. 1980, ApJL, 239, L107

Uchiyama, Y., et al. 2008, PASJ, 60, S35

Vasilopoulos, G., & Petropoulou, M. 2016, MNRAS, 455, 4426

Vaughan, S., et al. 2004, ApJ, 603, L5

Vaughan, S., et al. 2006, ApJ, 639, 323

Vianello, G., Tiengo, A., & Mereghetti, S. 2007, A&A, 473, 423

Xiang, J., Lee, J. C., Nowak, M. A. & Wilms, J. 2011, ApJ, 738, 78